# Linear Precoded Index Modulation

Hongming Zhang, *Member, IEEE*, Chunxiao Jiang, *Senior Member, IEEE*, Lie-Liang Yang, *Fellow, IEEE*, Ertugrul Basar, *Senior Member, IEEE*, and Lajos Hanzo, *Fellow, IEEE*

***Abstract*—Index modulation (IM) is an attractive concept for next generation communication systems. However, as an emerging technique, there are still some challenges need to be tackled in this frontier. In this paper, we consider two aspects of IM, which are diversity and detection complexity. Specifically, we propose a linear precoding assisted index modulation (LPIM) scheme for orthogonal frequency division multiplexing (OFDM) systems. We commence by analyzing the diversity and coding gains of the proposed scheme. Moreover, a detailed codebook design criterion is proposed. Then, our LPIM codebook is designed based on the maximum diversity and coding gain criteria. In contrast to the signaling model of the existing full diversity precoder designed for OFDM, we introduce a modeling method to link the zero-valued IM symbols to the origin of a Lattice for implementing our full diversity precoder designed for OFDM-IM. Both analytical and computer simulation results are provided for characterizing the attainable performance of OFDM-LPIM, demonstrating that it is capable of achieving full diversity as well as an attractive coding gain. However, the maximum-likelihood (ML) detection complexity of OFDM-LPIM is excessive, hence a low-complexity generalized iterative residual check detector (GIRCD) is proposed, which is inspired by the existing sparse recovery algorithms. Finally, computer simulation results are provided for demonstrating that GIRCD can provide a beneficial trade-off between bit error ratio performance and complexity.**

***Index Terms*—index modulation, OFDM, transmit diversity, algebraic number theory, greedy algorithm.**

## I. Introduction

INDEX modulation (IM) is a compelling candidate for 5G wireless networks [1–3]. Recently, orthogonal frequency-division multiplexing (OFDM) has been combined with IM (OFDM-IM) [4–6], where information is implicitly conveyed by the indices of the activated subcarriers and by the conventional amplitude-phase modulated (APM) symbols. As shown in [7–9], its flexibility in terms of striking a tradeoff between spectral efficiency (SE) and energy efficiency (EE) makes IM an attractive candidate for scenarios such as in-vehicle communications and device-to-device (D2D) communications [10] and wireless sensor networks.

However, as an emerging technique, there are some open research problems that require further investigation. First, the attainable SE of OFDM-IM is limited [8]. In [11], three types of OFDM schemes relying on generalized IM (OFDM-GIM) have been proposed to enhance the SE with the aid of the flexible selection of active subcarriers. Later in [9], a compressed sensing assisted IM scheme has been conceived for improving the attainable SE of the system. The dual-mode OFDM (DM-OFDM) technique has been proposed in [12] and [13], where all the subcarriers are encoded by IM schemes using different constellation modes, yielding an enhanced SE. Recently, multiple-mode OFDM-IM (MM-OFDM-IM) has been proposed in [14], which improves the SE with the aid of multiple constellation mode selection. Second, since information is conveyed by both APM and index modulated symbols, the design of a low-complexity detector, which provides a good detection performance, is challenging. In [6], a joint maximum-likelihood (JML) detector has been proposed by Basar *et al.* for OFDM-IM. Based on the fact that the frequency-domain (FD) symbols can be either zero or non-zero valued, the same authors have proposed a log-likelihood ratio (LLR) based detector, whose complexity has been shown to be lower than the JML detector [6]. Further improvements have been made in [15] for both the JML and LLR detectors. On the other hand, as demonstrated in [6, 16], the bit error ratio (BER) performance of the OFDM-IM system is better than that of OFDM using quadrature amplitude modulation (QAM), for a SE lower than 2 bits/s/Hz. Hence, it is important to improve the BER performance of the OFDM-IM scheme in the practically important high SE regime. In [17], the BER performance of the OFDM-IM scheme is improved by employing a symbol interleaver. Later in [15], a transmit diversity scheme, namely the coordinate interleaved orthogonal design [18], has been integrated to OFDM-IM systems to improve the BER performance. In [19], a beneficial transmit diversity gain was attained by transmitting the same information over both the active and inactive subcarriers of OFDM-IM. The authors of [20] proposed a constellation rotation scheme for gleaning an improved diversity gain for OFDM-IM. Recently, generalized analytical results of the achievable diversity order of OFDM-IM systems have been provided in [9], showing that the attainable multipath diversity gain has not been achieved by the aforementioned schemes. In order to gain insights into the design of full diversity schemes for OFDM-IM, we review some of the existing works in the following.

For transmission over multipath propagation channels, one of the most powerful contributors to reliable communications is the diversity, including modulation diversity, temporal diversity, frequency diversity and space diversity, as detailed in [21, 22]. During the last two decades, considerable research attention has been paid to the context of diversity, especially to multiple-input-multiple-output (MIMO) scenarios, to name but a few [21, 23–28]. In this paper, we limit ourselves to diversity techniques conceived for OFDM systems. We shall emphasize that both MIMO and OFDM signaling schemes share the same mathematical fundamentals in the context of diversity invoked for combating channel fading. The early contribution in [22] has demonstrated that the BER performance of fading channels approaches that of the Gaussian channels, when the

L. Hanzo gratefully acknowledges the financial support of the EPSRC projects EP/Noo4558/1, EP/PO34284/1, of the Royal Society as well as of the European Research Council's Advanced Fellow Grant QuantCom.

diversity order tends to infinity. On the other hand, it is widely discussed in [29] that a high bandwidth efficiency can be achieved by signal constellations having a lattice structure, such as the classic QAM scheme. Indeed, lattices from algebraic number fields serve as the theoretical foundations for the design of full-diversity codes. Accordingly, various constellation-rotation based modulation diversity approaches have been proposed, such as those given in [22, 23, 30, 31]. Specifically, the authors of [30] proposed a linear constellation precoded OFDM (LCP-OFDM) system for maximizing both the achievable diversity gain and the coding gain. However, the above-mentioned sophisticated approaches rely on high-complexity ML detection of full diversity codes at the receiver side. Later in [32], Liu demonstrated that a beneficial multipath diversity gain can be attained by single-carrier frequency-division multiple access (SC-FDMA), when an FD equalizer is employed between an IFFT/FFT pair. In [30], an optimal symbol interleaver, which relies on FD subcarrier grouping, was designed as a means of further increasing the coding gain of a precoded OFDM system. Later, the subcarrier grouping based symbol interleaving has been extensively investigated in [25, 33]. In particular, the authors of [25] demonstrated that in comparison to random permutation, about 1-3 dB performance gain can be achieved by the optimal design of the subcarrier grouping based symbol interleaver. For additional details, we refer interested readers to [33, 34]. As a further advance in the field, Xia *et al* proposed cyclotomic lattices for modeling the full diversity codes in [24], yielding a generalized optimal design for the existing classical modulation constellations, such as QAM and phase-shift keying (PSK). Recently, a new theorem has been developed in [35] to simplify the asymptotic analyses of diversity receptions over correlated lognormal fading channels, making it possible to evaluate outage probability of the diversity reception systems without resorting to time-consuming Monte Carlo simulation or multi-fold numerical integration. However, to the best of authors' knowledge, this design philosophy has not been applied to the IM scheme, which has been recently recognized as a beneficial modulation scheme [9]. Specifically, in comparison to the existing classical modulation formats, such as QAM and PSK, the IM scheme contains inactive symbols, which are zero-valued, in each group. As a benefit, the power saved this way may be assigned to the activated symbols to avoid a throughput loss. Hence, it is challenging to design a full-diversity precoder for such a multidimesional sparse signal set in order to achieve a good error performance.

*To address the aforementioned issues, the contributions of this paper are summarized as follows:*

- *We propose a linear transmit pre-coding assisted IM codebook, namely our linear precoding assisted index modulation (LPIM) codebook for short, based on the maximization of the diversity gain and the coding gain as our design criteria. We first model the IM symbols as lattice points from the ring of Gaussian integers. Specifically, we model the zero-valued IM symbols as the origin of a Lattice. Then, based on algebraic number theory, an optimal linear precoding matrix is introduced for the IM scheme. Furthermore, the optimality in terms of achieving the maximum attainable diversity order of the proposed scheme is proved for such a multidimesional sparse signal set. As a further improvement, a symbol interleaver is conceived for improving the coding gain of the OFDM using LPIM (OFDM-LPIM) system. Both analytical and computer simulation results are provided for characterizing the overall performance of the OFDM-LPIM system. It is demonstrated that the proposed OFDM-LPIM system is capable of achieving the maximum attainable diversity gain as well as coding gain, hence yielding a significant BER performance improvement. Furthermore, in some scenarios, the OFDM-LPIM system is capable of attaining a better BER performance than the OFDM system relying on a full-diversity precoder.*
- *We first invoke the JML detection for our proposed OFDM-LPIM scheme for the sake of performance comparison. Then, a low-complexity detector, namely the generalized iterative residual check detector (GIRCD), is proposed for the OFDM-LPIM systems. Specifically, GIRCD is a further development of the sparse symbol detector proposed in [9]. The philosophy is based on the greedy algorithms developed for sparse recovery, where the global optimum is approximated by iteratively updating estimates that are obtained by making locally optimal choices at each step.*

The rest of the paper is organized as follows. In Section II, our system model is described. Then, the system performance analysis and codebook design criteria are detailed in Section III. In Section IV, we propose our LPIM codebook design. In Section V, the GIRCD is proposed. Our simulation results are discussed in Section VI. Finally, we offer our conclusions in Section VII.

*Notation:* We use the following notation throughout this paper: $\mathbb{B}$ is the bit set containing $\{0, 1\}$. $\mathbb{R}$, $\mathbb{C}$, $\mathbb{Q}$ and $\mathbb{Z}$ stand for the ring of real, complex, rational and integer numbers, respectively, and $\mathbb{Z}_+^N$ is a set of real integers containing $\{1, 2, \ldots, N\}$. The ring of Gaussian integers is denoted by $\mathbb{Z}[j]$, which is defined as $\mathbb{Z}[j] \triangleq \{a + jb : a, b \in \mathbb{Z}\}$, while $\mathbb{Z}[\omega]$ denotes the ring of Eisenstein integers, which is defined as $\mathbb{Z}[\omega] \triangleq \{a + \omega b : a, b \in \mathbb{Z}\}$ with $\omega = \exp(j2\pi/3)$. $\mathbb{Q}(\alpha_P)$ is the cyclotomic field with $\alpha_P$ being a primitive $P$th root of unity in $\mathbb{C}$. Matrices and vectors are denoted by upper- and lower-case boldface letters, respectively. $\boldsymbol{x}_{\mathrm{T}}$ and $\boldsymbol{x}_{\mathrm{F}}$ represents the time-domain (TD) and FD symbols, respectively. Furthermore, $\boldsymbol{x}(l)$ and $x(m, l)$ denote the $l$th block of symbols and the $m$th symbol of the $l$th block, respectively. $\mathcal{CN}(\boldsymbol{a}, \boldsymbol{B})$ denotes the complex Gaussian distribution with mean vector $\boldsymbol{a}$ and covariance matrix $\boldsymbol{B}$. $\mathbb{E}[\cdot]$ and $\mathcal{O}[\cdot]$ are the expectation operator and the big O operator, respectively. For a matrix $\boldsymbol{A}$, $(\boldsymbol{A})^T$, $(\boldsymbol{A})^*$, $(\cdot)^H$, and $(\cdot)^{-1}$ denotes its transpose, conjugate, conjugate transpose, and inverse, respectively. The $\ell_p$-norm and the pseudo-$\ell_0$-norm of a vector $\boldsymbol{x}$ is denoted as $\|\boldsymbol{x}\|_p$ and $\|\boldsymbol{x}\|_0$, respectively.

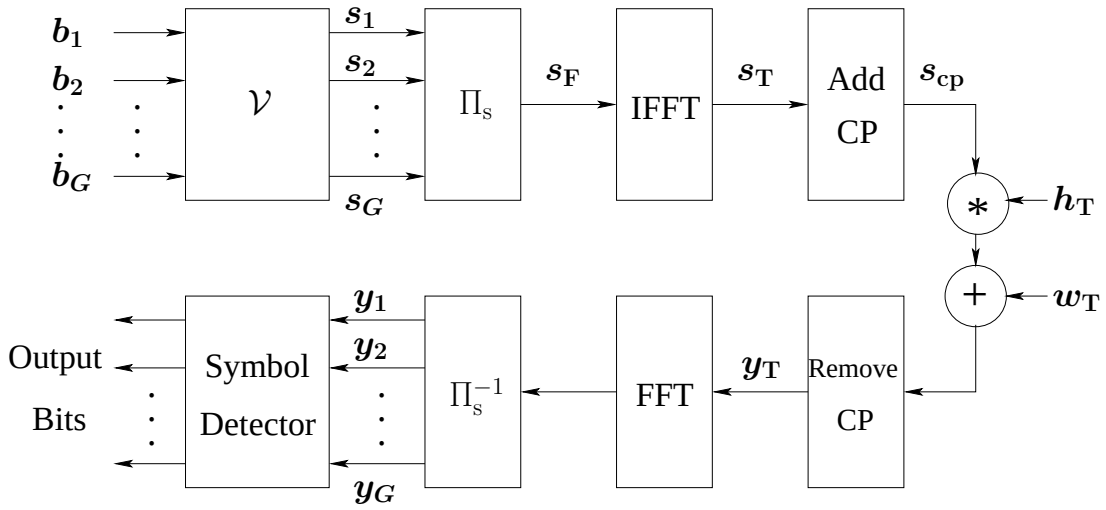


Fig. 1: Illustration of the OFDM system employing a codebook $\mathcal{V}$ and an interleaver $\Pi_{\rm s}$.

## II. System Model

### A. Transmitter Description

Let us consider an OFDM system consisting of $M$ subcarriers. Specifically, the $M$ subcarriers are uniformly divided into $G$ groups, where we have $G = 1, \ldots, M$. Hence, each group contains $m = M/G$ subcarriers. As seen in Fig. 1, the information bits in $\boldsymbol{b} \in \mathbb{B}^{LG}$ are first split into $G$ groups denoted as $\boldsymbol{b} = [\boldsymbol{b}_1, \ldots, \boldsymbol{b}_G]$, where we have $\boldsymbol{b}_g \in \mathbb{B}^L$ for $g = 1, \ldots, G$. As shown in [6], the conventional OFDM-IM scheme comprises an index mapper $\mu_1$ and an APM mapper $\mu_2$. Specifically, the bits in $\boldsymbol{b}_g$ are partitioned into two sub-sequences denoted as $\boldsymbol{b}_{1,g} \in \mathbb{B}^{L_1}$ and $\boldsymbol{b}_{2,g} \in \mathbb{B}^{L_2}$, where we have $L = L_1 + L_2$. The bits in $\boldsymbol{b}_{1,g}$ are mapped into an index symbol $\mathcal{I}_g$ according to $\mu_1 : \mathbb{B}^{L_1} \to \mathcal{Z}$, where $\mathcal{Z} = \{\mathcal{Z}_1, \ldots \mathcal{Z}_C\}$ contains $C = 2^{L_1}$ index subsets, each of which is formed by considering the selection of $k$ indices from $m$ indices. Thereby, we have $L_1 = \log_2 C = \lfloor \log_2 \binom{m}{k} \rfloor$. Let us denote the $c$th index subset of $\mathcal{Z}$ as $\mathcal{Z}_c = \{\mathcal{Z}_c(0), \ldots, \mathcal{Z}_c(k-1)\} \subset \mathcal{Z}$, where $\mathcal{Z}_c(i) \in \mathbb{Z}_+^N$ for $i = 0, \ldots, k-1$. Clearly, when the $g$th group of data bits is mapped into the $c$th candidate in $\mathcal{Z}$, we have $\mathcal{I}_g = \mathcal{Z}_c \subset \mathcal{Z}$. On the other hand, the bits in $\boldsymbol{b}_{2,g}$ are mapped onto $k$ APM symbols based on $\mu_2 : \mathbb{B}^{\log_2 Q} \to \mathcal{A}$, where $\mathcal{A} \triangleq \{a_1, \ldots, a_Q\}$ is the constellation alphabet of a $Q$-ary QAM/PSK scheme. Hence, we have $L_2 = k \log_2 Q$. Let us denote the $g$th group of APM symbols as $\boldsymbol{x}_{{\rm d},g} = [x_{{\rm d},g}(0), \ldots, x_{{\rm d},g}(k-1)]^T$, where it is assumed that $\mathbb{E}[|x_{{\rm d},g}(i)|^2] = 1$, $\forall x_{{\rm d},g}(i) \in \mathcal{A}$. Then, the symbols in $\boldsymbol{x}_{{\rm d},g}$ are respectively assigned to $k$ active subcarriers according to the indices in $\mathcal{I}_g$, yielding the $g$th group of symbols $\boldsymbol{x}_g = [x_g(0), \ldots, x_g(m-1)]^T$, which can be expressed as

$$\boldsymbol{x}_g = \boldsymbol{\Upsilon}_{\mathcal{I}_g} \boldsymbol{x}_{{\rm d},g}, \tag{1}$$

where $\boldsymbol{\Upsilon}_{\mathcal{I}_g}$ is an $(m \times k)$-element mapping matrix based on $\mathcal{I}_g$. Based on (1), a specifically designed precoding matrix $\boldsymbol{U} \in \mathbb{C}^{m \times m}$ is applied to $\boldsymbol{x}_g$, yielding

$$\boldsymbol{s}_g = \boldsymbol{U} \boldsymbol{x}_g, \tag{2}$$

where the precoding matrix $\boldsymbol{U}$ is assumed to be normalized so that we have $\mathbb{E}[\|\boldsymbol{s}_g\|_2^2] = \mathbb{E}[\|\boldsymbol{x}_g\|_2^2] = k$, $\forall g$. In particular, we assume that $\mathbb{E}[\|\boldsymbol{s}_g\|_2^2] = k \leq m$, $\forall g$. For the sake of demonstration, the above-mentioned bit-to-symbol mapping process of each group is assumed to be implemented according to a specifically designed codebook of

$$\mathcal{V} \triangleq \left\{ \boldsymbol{v}_1, \ldots, \boldsymbol{v}_{2^L} : \boldsymbol{v}_i \in \mathbb{C}^m, i = 1, \ldots, 2^L \right\}, \tag{3}$$

which will be detailed in Section IV. Next, all the $G$ groups of symbols are fed into an interleaver $\Pi_{\rm s}$ shown in Fig. 1, yielding the FD symbols expressed as $\boldsymbol{s}_{\rm F} = [s_{\rm F}(0), s_{\rm F}(1), \ldots, s_{\rm F}(M-1)]^T$. The design and discussions of the interleaver $\Pi_{\rm s}$ will be given in Section IV-B. For the sake of demonstration, let $\boldsymbol{\Upsilon}_{\Pi_g}$ represent the $(M \times m)$-element mapping matrix based on $\Pi_{\rm s}$ for the $g$th group. Furthermore, we can show that $\boldsymbol{\Upsilon}_{\Pi_g}^T \boldsymbol{\Upsilon}_{\Pi_g} = \boldsymbol{I}_m$ and $\boldsymbol{\Upsilon}_{\Pi_g}^T \boldsymbol{\Upsilon}_{\Pi_{g'}} = \boldsymbol{0}$ for $g' \neq g$. Hence, we express the FD symbols as

$$\boldsymbol{s}_{\rm F} = \sum_{g=1}^{G} \boldsymbol{\Upsilon}_{\Pi_g} \boldsymbol{s}_g, \tag{4}$$

which are processed by $M$-point IFFT, yielding the TD symbols $\boldsymbol{s}_{\rm T} = \boldsymbol{\mathcal{F}}_M^H \boldsymbol{s}_{\rm F}$, as seen in Fig. 1. Finally, after inserting a CP of length $L_{\rm cp}$, the transmitted baseband symbols can be written as $\boldsymbol{s}_{\rm cp} = \boldsymbol{\Upsilon}_{\rm CP}^T \boldsymbol{s}_{\rm T}$, where $\boldsymbol{\Upsilon}_{\rm CP} = [\boldsymbol{\Upsilon}_{\rm cp}, \boldsymbol{I}_M]$ and $\boldsymbol{\Upsilon}_{\rm cp}$ is the $(M \times L_{\rm cp})$-element mapping matrix, which is obtained from the last $L_{\rm cp}$ columns of the identity matrix $\boldsymbol{I}_M$.

### B. Received Signals

A perfect synchronization is assumed at the receiver. Meanwhile, the bandwidth of each subchannel is assumed to be much lower than the channels' coherence bandwidth. Let us consider an $L_{\rm h}$-tap frequency-selective Rayleigh fading channel, whose channel impulse response (CIR) is $\boldsymbol{h}_{\rm T} = [h_{\rm T}(0), h_{\rm T}(1), \ldots, h_{\rm T}(L_{\rm h}-1)]^T$, where the elements of $\boldsymbol{h}_{\rm T}$ are independent and identically distributed (i.i.d.) random variables that obey $\mathcal{CN}(0, 1/L_{\rm h})$. Here, we assume that $L_{\rm cp} \geq L_{\rm h}$. Then, as shown in Fig. 1, after the removal

of CP, the vector of received baseband equivalent signals $\boldsymbol{y}_{\mathrm{T}} = [y_{\mathrm{T}}(0), y_{\mathrm{T}}(1), \ldots, y_{\mathrm{T}}(M-1)]^T$ can be formulated as

$$\boldsymbol{y}_{\mathrm{T}} = \boldsymbol{H}_{\mathrm{cir}}\boldsymbol{s}_{\mathrm{T}} + \boldsymbol{n}_{\mathrm{T}}, \tag{5}$$

where $\boldsymbol{H}_{\mathrm{cir}} = \boldsymbol{\mathcal{F}}_M^H \boldsymbol{H} \boldsymbol{\mathcal{F}}_M \in \mathbb{C}^{M\times M}$ is a circulant matrix with $\boldsymbol{H} = \mathrm{diag}\{\sqrt{M}\boldsymbol{\mathcal{F}}_M \boldsymbol{\Upsilon}_{\mathrm{h}} \boldsymbol{h}_{\mathrm{T}}\}$, where $\boldsymbol{\Upsilon}_{\mathrm{h}}$ is an $(M \times L_{\mathrm{h}})$-element mapping matrix obtained by the first $L_{\mathrm{h}}$ columns of $\boldsymbol{I}_M$. In (5), $\boldsymbol{n}_{\mathrm{T}}$ is the vector of complex additive white Gaussian noise (AWGN) samples with zero mean and a covariance of $N_0\boldsymbol{I}_M$. As shown in Fig. 1, after the FFT operation and de-interleaving, the $g$th group of received FD symbols can be given as [9]

$$\boldsymbol{y}_g = \bar{\boldsymbol{H}}_g \boldsymbol{s}_g + \bar{\boldsymbol{n}}_g, \tag{6}$$

where by definition $\bar{\boldsymbol{n}}_g = \boldsymbol{\Upsilon}_{\Pi_g}^T (\boldsymbol{\mathcal{F}}_M \boldsymbol{n}_{\mathrm{T}})$ is the vector of $g$th group of de-interleaved FD noise samples. According to [9], the diagonal matrix $\bar{\boldsymbol{H}}_g$ in (6) can be written as

$$\bar{\boldsymbol{H}}_g = \mathrm{diag}\left\{\boldsymbol{F}_{\mathrm{h},\Pi_g}\boldsymbol{h}_{\mathrm{T}}\right\} = \mathrm{diag}\{\bar{h}_g(0), \ldots, \bar{h}_g(m-1)\}, \tag{7}$$

where $\boldsymbol{F}_{\mathrm{h},\Pi_g} = \sqrt{M}\boldsymbol{\Upsilon}_{\Pi_g}^T \boldsymbol{\mathcal{F}}_M \boldsymbol{\Upsilon}_{\mathrm{h}} \in \mathbb{C}^{m\times L_{\mathrm{h}}}$. Here, we can readily show that $\bar{h}_g(i) \sim \mathcal{CN}(0,1)$ and $\bar{n}_g(i) \sim \mathcal{CN}(0, N_0)$, $\forall g, i$. Therefore, the average SNR per symbol is given by

$$\gamma_s \triangleq \frac{\mathbb{E}[\|\boldsymbol{s}_g\|_2^2]}{\mathbb{E}[\|\bar{\boldsymbol{n}}_g\|_2^2]} = \frac{k}{mN_0}. \tag{8}$$

Finally, the conditioned probability density function (PDF) of $\boldsymbol{y}_g$ given $\boldsymbol{s}_g$ can be expressed as

$$p\left(\boldsymbol{y}_g|\boldsymbol{s}_g\right) = \frac{1}{(\pi N_0)^m} \exp\left\{-\frac{\|\boldsymbol{y}_g - \bar{\boldsymbol{H}}_g\boldsymbol{s}_g\|_2^2}{N_0}\right\}. \tag{9}$$

Typically, the optimum symbol detector for our system shown in Section II invokes the maximum *a posterior* (MAP) principle by solving the optimisation problem of

$$\boldsymbol{s}_g^{\mathrm{MAP}} = \arg\max_{\boldsymbol{v}_i \in \mathcal{V}} \left\{p\left(\boldsymbol{v}_i|\boldsymbol{y}_g\right)\right\}, \tag{10}$$

where $p\left(\boldsymbol{v}_i|\boldsymbol{y}_g\right)$ is the *a posteriori* probability of $\boldsymbol{v}_i$ given $\boldsymbol{y}_g$. Assuming that the candidates in $\mathcal{V}$ are independent and equiprobable, the MAP detector of (10) becomes equivalent to the ML detector, which can be expressed with the aid of (9) as

$$\boldsymbol{s}_g^{\mathrm{ML}} = \arg\min_{\boldsymbol{v}_i \in \mathcal{V}} \left\{\left\|\boldsymbol{y}_g - \bar{\boldsymbol{H}}_g\boldsymbol{v}_i\right\|_2^2\right\}. \tag{11}$$

## III. System Performance Analysis and Codebook Design Criteria

In this section, we analyze the system performance and the design criteria of the codebook $\mathcal{V}$. Throughout this section, we assume that the ML detection is performed with perfect channel state information at the receiver side (CSIR) for the sake of performance evaluation. We commence by deriving the SE and EE of the system. Then, the analytical results of the diversity and coding gain are detailed. Finally, we discuss the design criteria of the codebook $\mathcal{V}$.

### A. Diversity and Coding Gains

First, let us define the pairwise error event as $\{\boldsymbol{s}_g^{\mathrm{c}} \to \boldsymbol{s}_g^{\mathrm{e}}\}$, where $\boldsymbol{s}_g^{\mathrm{c}} = \boldsymbol{v}_i$ is the transmitted symbol vector, while $\boldsymbol{s}_g^{\mathrm{e}} = \boldsymbol{v}_j$ denotes the corresponding incorrect detection results obtained from (11), i.e. we have $\boldsymbol{v}_i \neq \boldsymbol{v}_j$ for $\boldsymbol{v}_i, \boldsymbol{v}_j \in \mathcal{V}$. Specifically, let us define $\mathcal{E} \triangleq \{\boldsymbol{e} = \boldsymbol{v}_j - \boldsymbol{v}_i : \boldsymbol{v}_i \neq \boldsymbol{v}_j, \forall \boldsymbol{v}_i, \boldsymbol{v}_j \in \mathcal{V}\}$. Then, according to [9], the average pairwise error probability (PEP) can be formulated as

$$P\left(\boldsymbol{s}_g^{\mathrm{c}} \to \boldsymbol{s}_g^{\mathrm{e}}\right) = \frac{1}{\pi}\int_0^{\frac{\pi}{2}} \prod_{i=1}^{V_{\mathrm{D}}} \left(1 + \frac{\lambda_i m\gamma_s}{4k\sin^2\theta}\right)^{-1} \mathrm{d}\theta, \tag{12}$$

where $\lambda_i$ denotes the nonzero eigenvalues of $\boldsymbol{D}_g = \boldsymbol{F}_{\mathrm{h},\Pi_g}^H \boldsymbol{E}^H \boldsymbol{E} \boldsymbol{F}_{\mathrm{h},\Pi_g} \in \mathbb{C}^{L_{\mathrm{h}}\times L_{\mathrm{h}}}$ for $\boldsymbol{E} = \mathrm{diag}\{\boldsymbol{e}\} \in \mathbb{C}^{m\times m}$ and $i = 1, \ldots, V_{\mathrm{D}}$, where according to [9], we have

$$V_{\mathrm{D}} = \min_{\forall \boldsymbol{e}\in\mathcal{E}} \{\|\boldsymbol{e}\|_0, L_{\mathrm{h}}\}. \tag{13}$$

Moreover, it can be shown that for sufficiently high SNR values, Eq.(12) is upper bounded by [21, 30]

$$P\left(\boldsymbol{s}_g^{\mathrm{c}} \to \boldsymbol{s}_g^{\mathrm{e}}\right) \leq \left(V_{\mathrm{C}}\frac{m\gamma_s}{4k}\right)^{-V_{\mathrm{D}}}, \tag{14}$$

where $V_{\mathrm{D}}$ denotes the diversity order of system with the ML detection, while

$$V_{\mathrm{C}} = \min_{\forall \Pi_s, \boldsymbol{e}\in\mathcal{E}} \left(\prod_{i=1}^{V_{\mathrm{D}}} \lambda_i\right)^{1/V_{\mathrm{D}}} \tag{15}$$

is the coding gain of the transmission scheme. Eq. (14) shows that the diversity order $V_{\mathrm{D}}$ determines how rapidly the average PEP decreases with the increasing values of SNR, while the coding gain $V_{\mathrm{C}}$ determines the SNR-shift of this PEP curve relative to a benchmark error rate curve of $(\gamma_s/4)^{-V_{\mathrm{D}}}$. Typically, it is desirable to design such a codebook $\mathcal{V}$ that the maximum diversity order can be achieved in order to combat multipath induced fading. When the maximum diversity order is achieved, the coding gain is expected to be maximized for further improving the system performance.

### B. Design Criteria of Codebook $\mathcal{V}$

Based on the above analysis, let us now discuss the design criteria invoked for the codebook $\mathcal{V}$. Specifically, three aspects are considered, which are described as follows.

*1) Diversity Gain Criterion:* Firstly, it can be readily inferred from (13) that the design of $\mathcal{V}$ with the goal of achieving the maximum diversity gain is equivalent to solving the optimization problem of

$$\mathcal{V}^{\mathrm{C1}} = \arg\max_{\mathcal{V}} V_{\mathrm{D}} = \arg\max_{\mathcal{V}} \left\{\min_{\forall \boldsymbol{e}\in\mathcal{E}} \{\|\boldsymbol{e}\|_0, L_{\mathrm{h}}\}\right\} \tag{16}$$

for $\|\boldsymbol{e}\|_0 \leq m$. Clearly, the solution of (16) is dependent on the minimum number of non-zero elements of the $m$-dimensional error vector $\boldsymbol{e} \in \mathcal{E}$, as discussed below.

The first case is when the number of channel taps $L_{\mathrm{h}}$ is fixed and known to the transmitter. In this case, the codebook $\mathcal{V}$ can be designed so that the condition of $m \geq \min_{\boldsymbol{e}\in\mathcal{E}} \|\boldsymbol{e}\|_0 \geq L_{\mathrm{h}}$ is satisfied, yielding the so-called maximum multipath diversity

gain of $L_{\rm h}$. Specifically, in slow fading scenarios, typically the maximum multipath diversity criterion is employed, since the transmitter is capable of acquiring *a priori* information about the CIR and hence $L_{\rm h}$. However, when the CIR changes rapidly over time, the transmitter becomes unable to collect reliable information concerning $L_{\rm h}$. In this case, the following design criterion may be preferred.

The second scenario is that the codebook $\mathcal{V}$ is designed so that only the equality of $\min_{\boldsymbol{e}\in\mathcal{E}} \|\boldsymbol{e}\|_0 = m$ is met. It should be noted that since $\|\boldsymbol{e}\|_0 \leq m$, this design criterion is equivalent to that of $\|\boldsymbol{e}\|_0 = m$ for any $\boldsymbol{e} \in \mathcal{E}$. Clearly, the ideal case is when the maximum multipath diversity gain is attained, i.e. we have $\|\boldsymbol{e}\|_0 = m = L_{\rm h}$, $\forall \boldsymbol{e} \in \mathcal{E}$, since in this case a beneficial tradeoff between the computational complexity and the performance gain can be struck. However, when the number of channel taps $L_{\rm h}$ is unknown, the dimension $m$ has to be sufficiently high in order to obtain as high a diversity gain as possible. The corresponding drawback is the resultant high complexity.

*2) Coding Gain Criterion:* Specifically, for the optimal codebook $\mathcal{V}^{\rm C1}$ of (16) associated with a maximum diversity order of $V_{\rm D,max}$, the $(L_{\rm h} \times L_{\rm h})$-element matrix $\boldsymbol{D}_g$ becomes of full rank. In this case, the product of the eigenvalues of $\boldsymbol{D}_g$, which is equal to its determinant denoted as $\det(\boldsymbol{D}_g)$, is nonzero-valued. Moreover, since the interleaver $\Pi_{\rm s}$ and the codebook $\mathcal{V}^{\rm C1}$ are independent, we can formulate the corresponding coding gain based on (15) as

$$\begin{aligned} V_{\rm C}^{\rm C1} &= \min_{\forall \boldsymbol{e}\in\mathcal{E}} \left[\det(\boldsymbol{D}_g)\right]^{\frac{1}{V_{\rm D,max}}} \\ &= \min_{\forall \boldsymbol{e}\in\mathcal{E}} \left[\det(\boldsymbol{F}_{{\rm h},\Pi_g}^H \boldsymbol{E}^H \boldsymbol{E} \boldsymbol{F}_{{\rm h},\Pi_g})\right]^{\frac{1}{V_{\rm D,max}}} \\ &= \min_{\forall g} \left[\det(\boldsymbol{F}_{{\rm h},\Pi_g}^H \boldsymbol{F}_{{\rm h},\Pi_g})\right]^{\frac{1}{V_{\rm D,max}}} \min_{\forall \boldsymbol{e}\in\mathcal{E}} \left[\det(\boldsymbol{E}^H \boldsymbol{E})\right]^{\frac{1}{V_{\rm D,max}}} \\ &\triangleq (\delta_\Pi^{\rm C1} \delta_\mathcal{E}^{\rm C1})^{\frac{1}{V_{\rm D,max}}}, \end{aligned} \tag{17}$$

where by definition, we have

$$\delta_\Pi^{\rm C1} \triangleq \min_{\forall g} \det(\boldsymbol{F}_{{\rm h},\Pi_g}^H \boldsymbol{F}_{{\rm h},\Pi_g}) \tag{18}$$

and

$$\delta_\mathcal{E}^{\rm C1} \triangleq \min_{\forall \boldsymbol{e}\in\mathcal{E}} \det(\boldsymbol{E}^H \boldsymbol{E}). \tag{19}$$

Specifically, for the codebook $\mathcal{V}^{\rm C1}$, one can show that $\boldsymbol{E} = {\rm diag}(\boldsymbol{e}) \in \mathbb{C}^{m\times m}$ is a full-rank diagonal matrix. In this case, we can rewrite (19) as

$$\delta_\mathcal{E}^{\rm C1} \triangleq \min_{\forall \boldsymbol{e}\in\mathcal{E}} \det(\boldsymbol{E}^H \boldsymbol{E}) = \min_{\forall \boldsymbol{e}\in\mathcal{E}} \prod_{i=1}^{m} |e(i)|^2, \tag{20}$$

which is known as the squared minimum product distance (MPD). Then, it can be readily inferred from (17) that maximizing the coding gain is equivalent to solving the joint optimization problems of

$$\begin{aligned} \left\{\Pi_{\rm s}^{\rm opt}, \mathcal{V}^{\rm C2}\right\} &= \arg\max_{\Pi_{\rm s}, \mathcal{V}^{\rm C1}} V_{\rm C}^{\rm C1} \\ &= \left\{ \arg\max_{\Pi_{\rm s}} \delta_\Pi^{\rm C1}, \arg\max_{\mathcal{V}^{\rm C1}} \delta_\mathcal{E}^{\rm C1} \right\}, \end{aligned} \tag{21}$$

yielding our design criterion for the interleaver $\Pi_{\rm s}$ and for the codebook $\mathcal{V}$, which can be formulated as

$$\Pi_{\rm s}^{\rm opt} = \arg\max_{\Pi_{\rm s}} \delta_\Pi^{\rm C1} \tag{22}$$

and

$$\mathcal{V}^{\rm C2} = \arg\max_{\mathcal{V}^{\rm C1}} \delta_\mathcal{E}^{\rm C1}, \tag{23}$$

respectively.

## IV. Linear Precoding Assisted Index Modulation

In this section, a linear precoding assisted index modulation (LPIM) codebook is proposed. Specifically, our LPIM codebook is designed based on the maximum diversity and coding gain criteria discussed in Section III-B. We commence by detailing our proposed LPIM codebook. Then, as a further improvement, the optimal design of the subcarrier interleaver $\Pi_{\rm s}$ is shown.

### A. Codebook Design

Specifically, the LPIM codebook denoted as $\mathcal{V}_{\boldsymbol{U}}$ is an implementation of $\mathcal{V}$ defined in (3). Additionally, we can show that since LP is achieved without reducing the transmission rate, the attainable rate of $\mathcal{V}_{\boldsymbol{U}}$ can be expressed as

$$\begin{aligned} R_{\mathcal{V}_{\boldsymbol{U}}} &= \frac{L}{m} = \frac{L_1 + L_2}{m} \\ &= \frac{1}{m}\left( \left\lfloor \log_2 \binom{m}{k} \right\rfloor + k \log_2 Q \right) \quad \text{bits/s/Hz}, \end{aligned} \tag{24}$$

which is fixed for the given values of $m$, $k$ and $Q$. Furthermore, it can be readily shown that the LPIM codebook design is equivalent to the design of the LP matrix $\boldsymbol{U}$ based on a given OFDM-IM scheme. Hence, by following the design criteria detailed in Section III-B, our LPIM codebook design is detailed below.

Firstly, let us consider the diversity gain criterion, as discussed in Section III-B1. Based on the pairwise error event $\{\boldsymbol{s}_g^{\rm c} \to \boldsymbol{s}_g^{\rm e}\}$ defined in Section III-A, let us express the error vector associated with (2) as

$$\boldsymbol{e} = \boldsymbol{s}_g^{\rm c} - \boldsymbol{s}_g^{\rm e} = \boldsymbol{U}\left(\boldsymbol{x}_g^{\rm c} - \boldsymbol{x}_g^{\rm e}\right), \tag{25}$$

where $\boldsymbol{x}_g^{\rm c}$ and $\boldsymbol{x}_g^{\rm e}$ denote the transmitted and the incorrect detection results of a symbol vector $\boldsymbol{x}_g$, respectively. As analyzed in (16), the diversity gain achieved by a codebook, e.g., say $\mathcal{V}_{\boldsymbol{U}}$, is dependent on the minimum number of non-zero elements in all the possible error vectors that can be obtained from the codebook $\mathcal{V}_{\boldsymbol{U}}$. Furthermore, we can infer from (25) that the number of non-zero elements in $\boldsymbol{e}$ is dependent on the uniqueness of the linear combination results of the activated symbols in $\boldsymbol{x}_g$. For example, let us assume that all elements in the symbol vector $\boldsymbol{s}_g$ of (2), which are obtained from the linear combinations of the activated symbols in $\boldsymbol{x}_g$, are unique. Then, we can readily show that the number of non-zero elements in all the possible error vectors related to $\boldsymbol{s}_g$ becomes identical to its dimension, i.e. we have $\|\boldsymbol{e}\|_0 = m, \forall \boldsymbol{s}_g^{\rm e} \in \mathcal{V}_{\boldsymbol{U}}$. By contrast, if there exists a symbol vector $\boldsymbol{x}_g^{\rm e} \neq \boldsymbol{x}_g^{\rm c}$ so that after the LP of (2), we have $\boldsymbol{s}_g^{\rm e} = \boldsymbol{s}_g^{\rm c}$ due to the unfavourable design of the

LP matrix $\boldsymbol{U}$. In this case, we have $\|\boldsymbol{e}\|_0 = 0$ for $\boldsymbol{s}_g^{\mathrm{c}}$, since the same results are obtained by the linear combinations of the activated symbols in $\boldsymbol{x}_g^{\mathrm{e}}$ and $\boldsymbol{x}_g^{\mathrm{c}}$. Here, we are interested in the former case, which leads to a codebook resulting in the maximum diversity gain. Similar design issues have been investigated in [22–25, 29, 30, 36]. Specifically, we adopt the cyclotomic lattice design scheme studied in [23, 24, 29], where the precoding matrix $\boldsymbol{U}$ is treated as the generator matrix of an $m$-dimensional complex lattice constructed from the cyclotomic field $\mathbb{Q}(\alpha_P)$, with $\alpha_P = \exp(j2\pi/P)$ being a primitive $P$th root of unity in the complex field $\mathbb{C}$. In more detail, the $(m \times m)$-element generator matrix $\boldsymbol{U}$ is defined as (35) shown at the top of this page, which is the product of a diagonal matrix multiplied by a Vandermonde matrix having a normalization factor of $1/\sqrt{m}$. In (35), the diagonal elements $\{\alpha_P^{p_1}, \alpha_P^{p_2}, \ldots, \alpha_P^{p_m}\}$ are the roots of the minimal polynomial of $\alpha_P$, where we have $p_1 = 1$ for $\alpha_P = \alpha_P^{p_1}$ and $\gcd(p_i, P) = 1$ for $i = 1, \ldots, m$. Furthermore, we will also show that the first row of the Vandermonde matrix of (35), which becomes $\left[1, \alpha_P, \alpha_P^2, \ldots, \alpha_P^{m-1}\right]$ for $p_1 = 1$, is a basis of the cyclotomic field $\mathbb{Q}(\alpha_P)$. Hence, based on Theorem 2 of [24], we have the following results

**Proposition 1.** *The codebook $\mathcal{V}_{\boldsymbol{U}}$ associated with the LP matrix of* (35) *achieves the full diversity order.*

*Proof:* See Appendix. ∎

Next, let us consider the coding gain design criterion of the codebook $\mathcal{V}_{\boldsymbol{U}}$. More particularly, we assume that the maximum diversity gain is achieved by employing the LP matrix of (35) in the following analysis. Firstly, based on (25), the squared MPD of (20) can be rewritten as

$$\begin{aligned}\delta_{\mathcal{E}}^{\mathrm{C1}} &= \min_{\forall \boldsymbol{e} \in \mathcal{E}} \prod_{i=1}^{m} |e(i)|^2 \\ &= \min_{\forall \boldsymbol{x}_g} \prod_{i=1}^{m} \left| \sum_{t=1}^{m} u_{i,t} \left[ x_g^{\mathrm{c}}(t) - x_g^{\mathrm{e}}(t) \right] \right|^2, \end{aligned} \tag{36}$$

where $u_{i,t}$ denotes the entry in the $i$th row and $t$th column of $\boldsymbol{U}$. Then, for a given QAM/PSK constellation, the parameters of the LP matrix given in (35) are obtained so that the corresponding coding gain can be maximized. Hence, the optimal LP matrix can be finally obtained by solving the optimization problem of

$$\begin{aligned}\mathcal{V}_{\boldsymbol{U}}^{\mathrm{C2}} &= \arg\max_{\boldsymbol{U}} \delta_{\mathcal{E}}^{\mathrm{C1}} \\ &= \arg\max_{\{P, p_2, \ldots, p_m\}} \min_{\forall \boldsymbol{x}_g} \prod_{i=1}^{m} \left| \sum_{t=1}^{m} u_{i,t} \left[ x_g^{\mathrm{c}}(t) - x_g^{\mathrm{e}}(t) \right] \right|^2, \end{aligned} \tag{37}$$

where, we have $u_{i,t} = \alpha_P^{tp_i}/\sqrt{m}$. On the other hand, observe in (17) that the coding gain of the system is also dependent on the design of the interleaver $\Pi_{\mathrm{s}}$, which is detailed next.

### B. Optimal Design of the Interleaver $\Pi_s$

Again, the interleaver $\Pi_{\mathrm{s}}$ governs the OFDM subcarriers grouping, which is usually characterized by $\delta_{\Pi}^{\mathrm{C1}}$ defined in (18). Furthermore, the optimal design of the interleaver $\Pi_{\mathrm{s}}$ can be obtained by solving the optimization problem of (22). As shown in [25, 30], the depth-$G$ interleaver of Fig. 2 permutes the $(m \times G)$-element input symbols by entering them on a column-by-column basis and outputting them on a row-by-row basis. Thus, the $(M \times m)$-element matrix $\boldsymbol{\Upsilon}_{\Pi_g}$ shown in (4) is characterized by $s_g(i) = s_{\mathrm{F}}(g-1+iG)$ for $g = 1, \ldots, G$ and $i = 0, 1, \ldots, m-1$. In this case, we have

$$\begin{aligned}\delta_{\Pi}^{\mathrm{C1}} &= \min_{\forall g} \det\left( \boldsymbol{F}_{\mathrm{h},\Pi_g}^H \boldsymbol{F}_{\mathrm{h},\Pi_g} \right) \\ &= \min_{\forall g} \det\left( \boldsymbol{\Upsilon}_{\mathrm{h}} \boldsymbol{\mathcal{F}}_M^H \boldsymbol{\Upsilon}_{\Pi_g} \boldsymbol{\Upsilon}_{\Pi_g}^T \boldsymbol{\mathcal{F}}_M \boldsymbol{\Upsilon}_{\mathrm{h}}^T \right) \\ &= \det\left( \boldsymbol{\Upsilon}_{\mathrm{h}} \boldsymbol{\mathcal{F}}_M^H \boldsymbol{\Upsilon}_{\Pi_1} \boldsymbol{\Upsilon}_{\Pi_1}^T \boldsymbol{\mathcal{F}}_M \boldsymbol{\Upsilon}_{\mathrm{h}}^T \right) = \ldots \\ &= \det\left( \boldsymbol{\Upsilon}_{\mathrm{h}} \boldsymbol{\mathcal{F}}_M^H \boldsymbol{\Upsilon}_{\Pi_G} \boldsymbol{\Upsilon}_{\Pi_G}^T \boldsymbol{\mathcal{F}}_M \boldsymbol{\Upsilon}_{\mathrm{h}}^T \right), \end{aligned} \tag{38}$$

which is a constant value for all groups due to the constant depth $G$ of the interleaver $\Pi_{\mathrm{s}}$.

### C. Complexity Analysis

In comparison to the conventional OFDM-IM scheme of [6], an additional complexity is imposed on both the transmitter and the receiver by our LPIM scheme. We point out here that the complexity of multiplications by zero-valued deactivated symbols can be neglected, since these operations can be avoided in practice. Bearing this in mind, let us detail the complexity associated with our LPIM codebook as follows.

First, at the transmitter side, upon substituting (1) into (2), we can infer that the complexity order of precoding each group of OFDM-IM symbols is given by $\mathcal{O}(k)$, i.e. by the computational cost of multiplying $k$ activated symbols with the corresponding entries in the LP matrix $\boldsymbol{U}$. Let us assume for a moment that the ML detection of (11) is employed at the receiver side. Hence, the corresponding complexity of detecting each group of LPIM symbols is dominated by searching through the space of all possible candidates in our LPIM codebook $\mathcal{V}_{\boldsymbol{U}}$, which is on order of $\mathcal{O}(2^L)$. Since we have $k \leq m < 2^L$, the overall complexity related to our LPIM codebook can be expressed with the aid of (24) as

$$\mathcal{O}(2^L) = \mathcal{O}\left( 2^{\lfloor \log_2 \binom{m}{k} \rfloor} Q^k \right). \tag{39}$$

Based on (39), we can show that for the case of $2 \leq k \leq m$, the overall complexity may become excessive even for a moderate constellation size of $Q$. Furthermore, it can be shown with the aid of (24) that there is a tradeoff between the achievable rate and the complexity of our LPIM scheme. Hence, in order to achieve a high rate, the corresponding detection complexity may become excessive.

## V. Generalized Iterative Residual Check Detector

In general, the complexity of the ML detector shown in Section II-B may be prohibitively excessive, even for a moderate-sized codebook $\mathcal{V}_{\boldsymbol{U}}$. In order to alleviate this problem, we propose a low-complexity detection scheme, namely GIRCD, in this section. We first discuss the generalized detection problems, and then, detail the proposed GIRCD. Throughout this section, the group index $g$ is neglected for notional brevity, since each group of received symbols is decoded in a similar way.

$$\boldsymbol{U}=\frac{1}{\sqrt{m}}\text{diag}\left\{\alpha_P^{p_1},\alpha_P^{p_2},\ldots,\alpha_P^{p_m}\right\}\begin{bmatrix}1 & \alpha_P^{p_1} & \alpha_P^{2p_1} & \ldots & \alpha_P^{(m-1)p_1}\\ 1 & \alpha_P^{p_2} & \alpha_P^{2p_2} & \ldots & \alpha_P^{(m-1)p_2}\\ \vdots & \vdots & \vdots & \ddots & \vdots\\ 1 & \alpha_P^{p_m} & \alpha_P^{2p_m} & \ldots & \alpha_P^{(m-1)p_m}\end{bmatrix}, \tag{35}$$

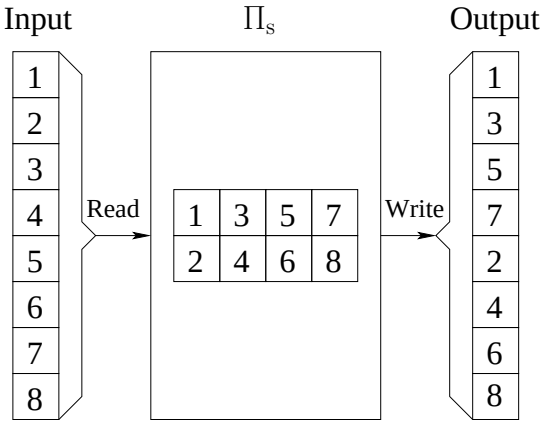


Fig. 2: Illustration of the interleaver $\Pi_{\text{s}}$ with a depth of $G=4$.

### A. Generalized Detection Problems

Based on Section IV, we can readily show that each group of received symbols can be formulated in a general way as

$$\begin{aligned}\boldsymbol{y}=&\boldsymbol{\Phi}\boldsymbol{x}+\bar{\boldsymbol{n}} &\text{(40a)}\\ =&\boldsymbol{\Phi}\boldsymbol{\Upsilon}_{\mathcal{I}}\boldsymbol{x}_{\text{d}}+\bar{\boldsymbol{n}} &\text{(40b)}\\ =&\boldsymbol{\Phi}_{\mathcal{I}}\boldsymbol{x}_{\text{d}}+\bar{\boldsymbol{n}}, &\text{(40c)}\end{aligned}$$

where by definition, we have $\boldsymbol{\Phi}_{\mathcal{I}}=\boldsymbol{\Phi}\boldsymbol{\Upsilon}_{\mathcal{I}}\in\mathbb{C}^{m\times k}$ with $\boldsymbol{\Phi}\in\mathbb{C}^{m\times m}$ defined as $\boldsymbol{\Phi}\triangleq\bar{\boldsymbol{H}}\boldsymbol{U}$. We assume that the index symbols in $\mathcal{Z}$ and the conventional APM symbols in $\mathcal{A}$ are independent and equiprobable. Hence, the conditional PDF of $\boldsymbol{y}$ can be formulated based on (9) and (40) as

$$\begin{aligned}p\left(\boldsymbol{y}|\boldsymbol{x}\right)=&p\left(\boldsymbol{y}|\boldsymbol{\Upsilon}_{\mathcal{I}}\boldsymbol{x}_{\text{d}}\right)=p\left(\boldsymbol{y}|\mathcal{I},\boldsymbol{x}_{\text{d}}\right)\\ =&\frac{1}{(\pi N_0)^m}\exp\left\{-\frac{\|\boldsymbol{y}-\boldsymbol{\Phi}\boldsymbol{\Upsilon}_{\mathcal{I}}\boldsymbol{x}_{\text{d}}\|_2^2}{N_0}\right\},\end{aligned} \tag{41}$$

which yields the JML detection of

$$\left(\mathcal{I}^{\text{ML}},\boldsymbol{x}_{\text{d}}^{\text{ML}}\right)=\underset{\mathcal{Z}_c\subset\mathcal{Z},\boldsymbol{a}\in\mathcal{A}^k}{\arg\min}\left\{\|\boldsymbol{y}-\boldsymbol{\Phi}\boldsymbol{\Upsilon}_{\mathcal{Z}_c}\boldsymbol{a}\|_2^2\right\}, \tag{42}$$

where $\boldsymbol{\Upsilon}_{\mathcal{Z}_c}$ is a mapping matrix based on $\mathcal{Z}_c$. In order to detect the IM symbols and APM symbols at an even low-complexity, below we propose GIRCD.

### B. Generalized Iterative Residual Check Detector

The basic idea of GIRCD is inspired by the principle of greedy algorithms developed for sparse recovery, e.g. [37, 38], where an approximated estimate is obtained by making locally optimal choices at each step. Specifically, our GIRCD is composed of two stages, an index reliability measure stage and an iterative detection stage, as detailed below.

At the index reliability measure stage, a soft estimate $\hat{\boldsymbol{x}}$ for $\boldsymbol{x}$ is obtained from the observation vector $\boldsymbol{y}$ in (40a) by invoking the linear minimum mean square error (LMMSE) processing, yielding

$$\hat{\boldsymbol{x}}=\left(\boldsymbol{\Phi}^H\boldsymbol{\Phi}+\frac{1}{\gamma_s}\boldsymbol{I}_m\right)^{-1}\boldsymbol{\Phi}^H\boldsymbol{y}, \tag{43}$$

where $\hat{\boldsymbol{x}}=[\hat{x}(0),\ldots,\hat{x}(m-1)]^T\in\mathbb{C}^m$. With high probability, the elements in $\hat{\boldsymbol{x}}$ with high magnitudes correspond to the active elements in $\boldsymbol{x}$, which becomes more evident when the SNR is high. Therefore, similar to [39], the reliability measure of index symbols can be obtained by ordering the magnitudes of elements in $\hat{\boldsymbol{x}}$ in descending order as

$$\begin{aligned}&\{i_1,i_2,\ldots,i_m\}\text{ subject to}\\ &\qquad|\hat{x}(i_1)|^2\geq|\hat{x}(i_2)|^2\geq\ldots\geq|\hat{x}(i_m)|^2,\end{aligned} \tag{44}$$

where we have $i_j\in\{0,\ldots,m-1\}$ for $j=1,\ldots,m$ and $i_j\neq i_q$ for any $j\neq q$. We shall emphasize here that our GIRCD simply treats the index $i_1$ as the candidate with highest priority to be tested in the following iterative detection stage, rather than a detection result of an index symbol in $\mathcal{I}$. With the aid of this preparation, GIRCD forwards to the next stage, where both the conventional APM and index symbols are detected, as detailed below.

During the second stage, GIRCD first selects candidates from the index codebook $\mathcal{Z}$ based on the index $i_t$ shown in (44), since it has the highest priority to be tested at the $t$th iteration. In detail, let the selected candidates be grouped into a candidate space denoted as $\mathcal{Z}^t$ for the $t$th iteration, which can be expressed as

$$\mathcal{Z}^t=\{\mathcal{Z}_1^t,\mathcal{Z}_2^t,\ldots,\mathcal{Z}_{C_t}^t\}\subset\mathcal{Z} \tag{45}$$

where $C_t$ denotes the number of candidates at the $t$th iteration and $\mathcal{Z}_{c_t}^t(i)\in\mathbb{Z}_+^N$ for $i=0,\ldots,k-1$. Here, all the selected candidates contain the index $i_t$ as one of their members, i.e., we have $\bigcap_{c_t=1}^{C_t}\mathcal{Z}_{c_t}^t=i_t$. Then, based on the candidate $\mathcal{Z}_{c_t}^t$, which is treated as the *a priori* information for the following activated symbol detection, the corresponding local optimal results can be obtained with the aid of (40c) by solving the optimization problem of

$$\breve{\boldsymbol{x}}_{\text{d}}(c_t)=\underset{\boldsymbol{v}\in\mathbb{C}^{k\times1}}{\arg\min}\left\|\boldsymbol{y}-\boldsymbol{\Phi}_{\mathcal{Z}_{c_t}^t}\boldsymbol{v}\right\|_2^2, \tag{46}$$

which can be solved by the well-known ordinary least square approach, giving

$$\begin{aligned}\breve{\boldsymbol{x}}_{\text{d}}(c_t)=&\boldsymbol{\Phi}_{\mathcal{Z}_{c_t}^t}^{\dagger}\boldsymbol{y}=\boldsymbol{\Phi}_{\mathcal{Z}_{c_t}^t}^{\dagger}\boldsymbol{\Phi}_{\mathcal{I}}\boldsymbol{x}_{\text{d}}+\boldsymbol{\Phi}_{\mathcal{Z}_{c_t}^t}^{\dagger}\bar{\boldsymbol{n}}\\ =&\boldsymbol{x}_{\text{d}}+\boldsymbol{r}_{\mathcal{I},\mathcal{Z}_{c_t}^t}+\breve{\boldsymbol{n}},\end{aligned} \tag{47}$$

where $\boldsymbol{\Phi}_{\mathcal{Z}_{c_t}^t}^{\dagger}$ denotes the Moore-Penrose pseudoinverse matrix of $\boldsymbol{\Phi}_{\mathcal{Z}_{c_t}^t}$ and $\boldsymbol{r}_{\mathcal{I},\mathcal{Z}_{c_t}^t}$ is the residual interference. Clearly, if the correct candidate is detected, we have $\boldsymbol{r}_{\mathcal{I},\mathcal{Z}_{c_t}^t}=\boldsymbol{0}$. In (47), the

noise vector $\breve{\boldsymbol{n}} = \boldsymbol{\Phi}^{\dagger}_{\mathcal{Z}^t_{c_t}} \bar{\boldsymbol{n}} \in \mathbb{C}^{k\times 1}$ is a Gaussian noise vector since it is a linear combination of Gaussian noise samples.

Next, GIRCD derives an APM candidate denoted as $\boldsymbol{a}^t(c_t) = [a^t(0,c_t),\ldots,a^t(k-1,c_t)]^T$ from the index candidate $\mathcal{Z}^t_{c_t}$ by carrying out a simple symbol-by-symbol ML detection expressed as

$$a^t(i,c_t) = \arg\min_{a_q\in\mathcal{A}} |\breve{x}_{\mathrm{d}}(i,c_t) - a_q|^2 \tag{48}$$

for $i = 0,\ldots,k-1$. Let all the $C_t$ APM candidates at the $t$th iteration be grouped into a set denoted as $\mathcal{A}^t = \{\boldsymbol{a}^t(1),\ldots,\boldsymbol{a}^t(C_t)\} \subset \mathcal{A}^k$. Then, the best one among them is found by solving the following optimization:

$$\left(\mathcal{I}^{[t]}, \boldsymbol{x}^{[t]}_{\mathrm{d}}\right) = \arg\min_{\mathcal{Z}^t_{c_t}\in\mathcal{Z}^t, \boldsymbol{a}^t(c_t)\in\mathcal{A}^t} \left\|\boldsymbol{y} - \boldsymbol{\Phi}_{\mathcal{Z}^t_{c_t}} \boldsymbol{a}^t(c_t)\right\|_2^2. \tag{49}$$

Consequently, we obtain the the residual error $\varepsilon^{[t]}$ as

$$\varepsilon^{[t]} = \left\|\boldsymbol{y} - \boldsymbol{\Phi}_{\mathcal{I}^{[t]}} \boldsymbol{x}^{[t]}_{\mathrm{d}}\right\|_2^2. \tag{50}$$

Finally, GIRCD terminates when the residual error $\varepsilon^{[t]}$ is not higher than a predefined threshold denoted as $\varepsilon_{\mathrm{TS}}$. In this case, the results given in (49) are taken as the detected IM symbol and the detected APM symbol, respectively. Note that, if the condition of $\varepsilon^{[t]} \le \varepsilon_{\mathrm{TS}}$ cannot be satisfied after the maximum affordable number of iterations, the results giving the minimum residual error are output. Our proposed GIRCD is summarized in Algorithm 1.

**Algorithm 1** Generalized Iterative Residual Check Detector

**Require:** $\boldsymbol{y}$, $\boldsymbol{\Phi}$, $\gamma_s$, $\mathcal{Z}$, $\varepsilon_{\mathrm{TS}}$

**Preparation**: Set the stopping iterations of $t_{\mathrm{stop}}$, a check space of $\mathcal{Z}_{\mathrm{check}} = \mathcal{Z}$, $\varepsilon_0 = \infty$, $\mathcal{I}^{\mathrm{GIRCD}} = \emptyset$ and $\boldsymbol{x}^{\mathrm{GIRCD}}_{\mathrm{d}} = \emptyset$.

LMMSE detection based on (43), realized as

$$\hat{\boldsymbol{x}} = \left(\boldsymbol{\Phi}^H\boldsymbol{\Phi} + \frac{1}{\gamma_s}\boldsymbol{I}_m\right)^{-1}\boldsymbol{\Phi}^H\boldsymbol{y};$$

Obtain the index reliability measures by descending the magnitudes of $\hat{\boldsymbol{x}}$ as

$$|\hat{x}(i_1)|^2 \ge |\hat{x}(i_2)|^2 \ge \ldots \ge |\hat{x}(i_m)|^2.$$

**for** $t = 1$ to $t_{\mathrm{stop}}$ **do**

  Obtain $\mathcal{Z}^t = \{\mathcal{Z}^t_1, \mathcal{Z}^t_2, \ldots, \mathcal{Z}^t_{C_t}\}$ from $\mathcal{Z}_{\mathrm{check}}$, where $\bigcap_{c_t=1}^{C_t} \mathcal{Z}^t_{c_t} = i_t$;

  **if** $\mathcal{Z}^t = \emptyset$ **then**

  **else**

    For $c_t = 1,\ldots,C_t$, compute

$$\breve{\boldsymbol{x}}_{\mathrm{d}}(c_t) = \boldsymbol{\Phi}^{\dagger}_{\mathcal{Z}^t_{c_t}} \boldsymbol{y};$$

    Obtain the APM candidates for $c_t = 1,\ldots,C_t$ according to (48) as

$$a^t(i,c_t) = \arg\min_{a_q\in\mathcal{A}} \left|\breve{x}_{\mathrm{d},g}(i,c_t) - a_q\right|^2, \quad i = 0,1,\ldots,k-1$$

    Find the locally optimal choice by considering (49) as

$$\left(\mathcal{I}^{[t]}, \boldsymbol{x}^{[t]}_{\mathrm{d}}\right) = \arg\min_{\mathcal{Z}^t_{c_t}\in\mathcal{Z}^t, \boldsymbol{a}^t(c_t)\in\mathcal{A}^t} \left\|\boldsymbol{y} - \boldsymbol{\Phi}_{\mathcal{Z}^t_{c_t}} \boldsymbol{a}^t(c_t)\right\|_2^2.$$

    Calculate the residual error based on (50) as

$$\varepsilon^{[t]} = \left\|\boldsymbol{y} - \boldsymbol{\Phi}_{\mathcal{I}^{[t]}} \boldsymbol{x}^{[t]}_{\mathrm{d}}\right\|_2^2;$$

    **if** $\varepsilon^{[t]}_g < \varepsilon_{\mathrm{TS}}$ **then**

      Update $\mathcal{I}^{\mathrm{GIRCD}} = \mathcal{I}^{[t]}$ and $\boldsymbol{x}^{\mathrm{GIRCD}}_{\mathrm{d}} = \boldsymbol{x}^{[t]}_{\mathrm{d}}$.

      **exit**

    **else if** $\varepsilon^{[t]}_g < \varepsilon_0$ **then**

      Update $\mathcal{Z}_{\mathrm{check}} = \mathcal{Z}_{\mathrm{check}} \backslash \mathcal{Z}^t$, $\varepsilon_0 = \varepsilon^{[t]}$, $\mathcal{I}^{\mathrm{GIRCD}} = \mathcal{I}^{[t]}$ and $\boldsymbol{x}^{\mathrm{GIRCD}}_{\mathrm{d}} = \boldsymbol{x}^{[t]}_{\mathrm{d}}$.

    **else**

    **end if**

  **end if**

**end for**

**return** $\mathcal{I}^{\mathrm{GIRCD}}$ and $\boldsymbol{x}^{\mathrm{GIRCD}}_{\mathrm{d}}$.

### C. Complexity Analysis

First, based on our analysis shown in Section IV-C, we can known that the complexity of the ML detection of each block of LPIM symbols is on the order of $\mathcal{O}(2^L)$, since the size of the search space is exponential in the blocklength of each code in $\mathcal{V}_{\boldsymbol{U}}$. Whilst, for the proposed GIRCD shown in Algorithm 1, the complexity cost is determined by the number of iterations as well as the number of candidates in each iteration. Specifically, the best case corresponds to the detection within a single iteration through testing only one candidate. In this case, it can be easily shown that the overall complexity is on the order of $\mathcal{O}(Qk)$. On the contrary, the worst case corresponds to the testing of candidates in the index codebook $\mathcal{Z}$. The corresponding complexity is given by $\mathcal{O}(2^{L_1}Qk)$ for this case. It should be noted that the detection complexity of GIRCD in the worst case is still lower than that of the ML detector, since a symbol-by-symbol ML detection shown in (48) is performed. In most cases, as it will be shown in Section VI, our GIRCD requires only a single iteration for testing about $C_1 < C = 2^{L_1}$ candidates. In this case, the detection complexity is on the order of $\mathcal{O}(C_1Qk)$.

## VI. Performance Results

In this section, computer simulation results are provided for characterizing the achievable performance of the proposed LPIM and GIRCD. For all computer simulations, we consider a ten-path (i.e. $L_{\mathrm{h}} = 10$) slow-varying Rayleigh fading channel, which is based on Section II-B. An OFDM system employing $M = 256$ subcarriers is assumed, where the CP length is $L_{\mathrm{cp}} = 16$. Furthermore, the depth-$G$ interleaver given in Section IV-B is employed.

The BER performance of classical OFDM, conventional OFDM-IM, OFDM with dual-mode index modulation (OFDM-DM-IM), OFDM with coordinate interleaving aided index modulation (OFDM-CI-IM), OFDM with linear precoding (OFDM-LP), as well as our OFDM-LPIM system is compared in Fig. 3 (a) and Fig. 3 (b). In these figures, all systems employ $M = 256$ subcarriers, which are detected by the ML detector of Section II-B. The LPIM codebook is designed based on Section IV-A, whilst the LP codebooks is obtained according to [24]. For the sake of comparison, $\eta M$ subcarriers are used for the transmission of QPSK symbols in the classical OFDM, yielding a transmission rate of $\eta \log_2 Q$ bits/s/Hz. Explicitly, we have $\eta = 0.5, 0.75, 1, 0.626$ for maintaining a transmission rate of $1.0, 1.5, 2.0, 2.5$ bits/s/Hz, respectively. Based on the simulation results of Fig. 3, we

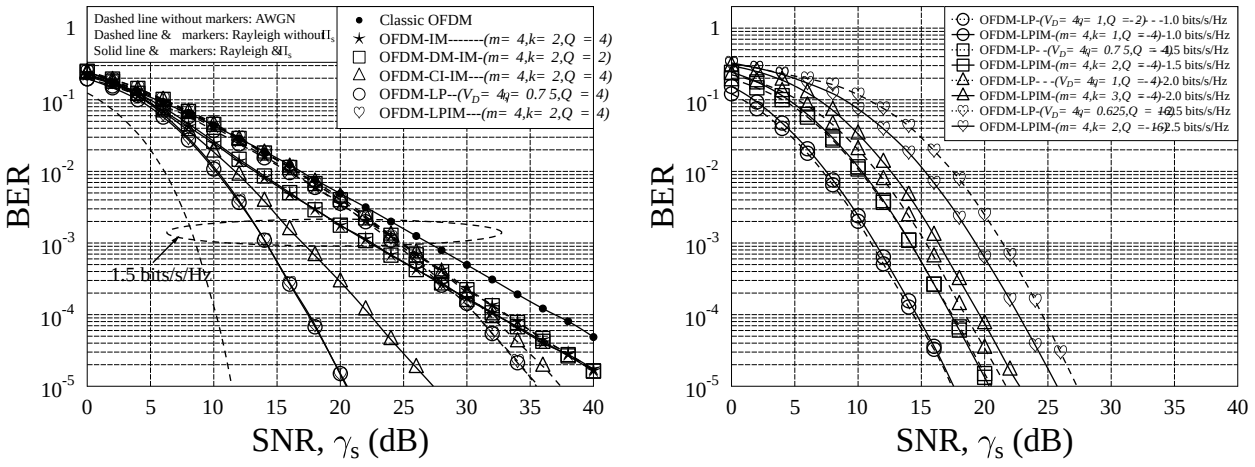


(a) (b)

Fig. 3: BER performance of the classical OFDM, the conventional OFDM-IM, the OFDM with dual-mode index modulation (OFDM-DM-IM), the OFDM with coordinate interleaving aided index modulation (OFDM-CI-IM), the OFDM with linear precoding (OFDM-LP), as well as our OFDM-LPIM systems employing $M = 256$ subcarriers and ML detection.

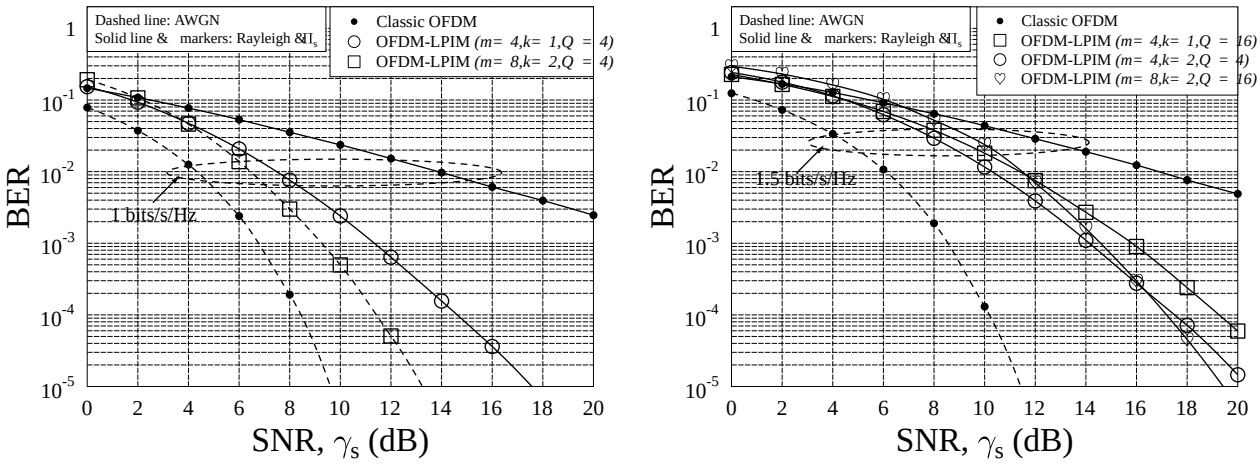


(a) (b)

Fig. 4: BER performance of the OFDM-LPIM system employing $M = 256$ subcarriers and ML detection, when communicating over an $L_{\rm h} = 10$-path Rayleigh fading channel. The OFDM-LPIM system uses the depth-$G$ interleaver $\Pi_{\rm s}$.

have the following observations. Firstly, the system performance of OFDM-IM, OFDM-DM-IM, OFDM-CI-IM, OFDM-LP, as well as OFDM-LPIM systems using the depth-$G$ interleaver is better than those without using interleaving, respectively. This is because that the depth-$G$ interleaver shown in Section IV-B provides an additional coding gain, hence yielding a much better error performance. Secondly, for a given maximum achievable rate, our proposed OFDM-LPIM scheme significantly outperforms the classical OFDM, the conventional OFDM-IM, OFDM-DM-IM, OFDM-CI-IM scheme for multipath fading channels. This observation can be explained with the help of our analysis in Section III-A. As proved in Proposition 1 of Section IV-A, the diversity order of our OFDM-LPIM system is $V_{\rm D} = m$, which is higher than that of the classical OFDM, OFDM-IM, OFDM-DM-IM, as well as the OFDM-CI-IM scheme. Thus, a much better error performance can be obtained by our OFDM-LPIM system. Thirdly, observe from Fig. 3 (b) that the BER performance of the OFDM-LPIM system is slightly worse than that of the OFDM-LP system for $\eta = 1$. This is because the MPD $\delta_{\mathcal{E}}^{\rm C1}$ shown in (20) attained by the linear precoded APM signalling is higher than that attained by the LPIM signalling. Thus,

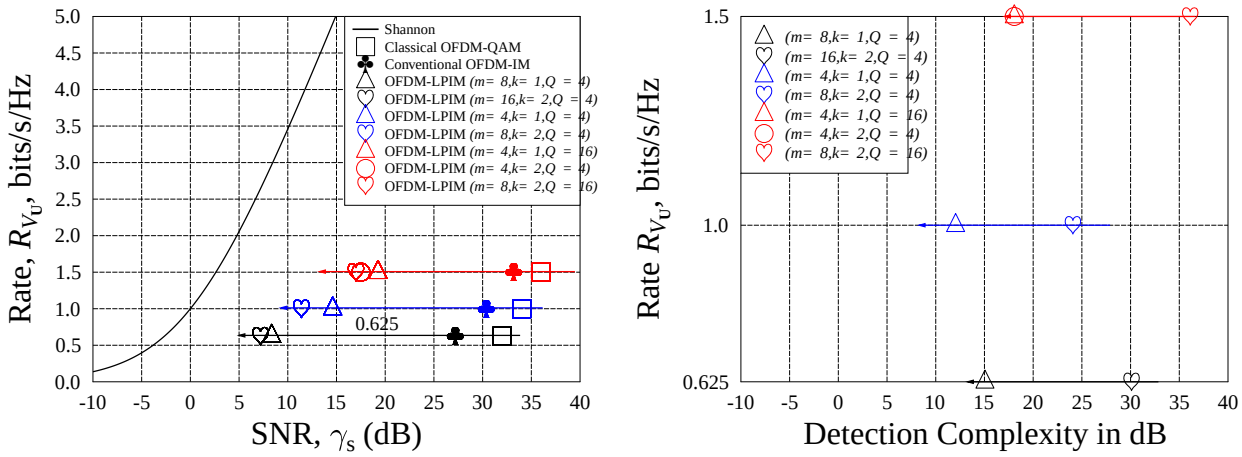


(a) The rate versus SNR per symbol at the BER of $10^{-4}$

(b) The rate versus detection complexity

Fig. 5: Performance of the OFDM-LPIM systems employing the depth-$G$ interleaver $\Pi_s$. The system parameters are given in Table I, where the maximum achievable rate $R_{\mathcal{V}_U}$ is obtained according to (24).

TABLE I: The Analytical Results of the LPIM Codebooks

| Rate $R_{\mathcal{V}_U}$ in bits/s/Hz | Codebook Parameters $(m, k, Q)$ | Diversity Gain | Coding Gain in dB |
|---|---|---|---|
| 1.0 | $(4, 1, 4)$ | 4 | -20.1916 |
| | $(8, 2, 4)$ | 8 | -23.3298 |
| 1.5 | $(4, 1, 16)$ | 4 | -27.1813 |
| | $(4, 2, 4)$ | 4 | -20.1916 |
| | $(8, 2, 16)$ | 8 | -30.3195 |

a better BER performance can be achieved by the OFDM-LP system, when $\eta = 1$. Finally, the proposed OFDM-LPIM outperforms the OFDM-LP scheme for $\eta < 1$. Moreover, the lower the value of $\eta$, the higher the performance gain attained by our OFDM-LPIM system. Since some subcarriers are not used for data transmission in the OFDM-LP systems having $\eta < 1$, the channel information cannot be fully exploited for the ML detection at the receiver side. Furthermore, the loss of channel information becomes more severely as the value of $\eta$ decreases. Hence, the coding gain attained by the interleaver $\Pi_s$ shown in Section IV-B is reduced. Therefore, the attainable BER performance of OFDM-LP systems is degraded.

In Fig. 4 (a) and Fig. 4 (b), the BER performance of the proposed OFDM-LPIM system is investigated. In these figures, all systems employ $M = 256$ subcarriers, which are detected by the ML detector of Section II-B. The related parameters and the analytical results of the OFDM-LPIM systems are summarized in Table I. Note that the corresponding analytical results are obtained based upon substituting the results of (36) and (38) into (17). The LPIM codebook is designed based on Section IV-A. Based on the simulation results of Fig. 4, we have the following observations. Firstly, we can observe from Fig. 3 that for a given maximum achievable rate, the higher the diversity order of the LPIM codebook, the better the BER performance of the system. Secondly, as shown in Fig. 4, when the achievable rate and the diversity order are fixed, the lower the constellation size of the activated symbols, the better the BER performance becomes. This is because a low constellation size exhibits a high minimum distance for the codebook. In this case, the corresponding squared MPD $\delta_{\mathcal{E}}^{\mathrm{C1}}$ shown in (36) is high. This can be readily verified by our analytical results of the coding gain shown in Table I, where for a given maximum achievable rate of 1.5 bits/s/Hz, the coding gain of the LPIM associated with $(m = 4, k = 2, Q = 4)$ is about 6.5 dB higher than that of the LPIM using $(m = 4, k = 1, Q = 16)$. As a result, the coding gain of the codebook obtained from (17) is high, hence yielding a good BER performance.

In Fig. 5, we investigate the performance of the proposed OFDM-LPIM system employing the depth-$G$ interleaver $\Pi_s$. The related parameters are given in Table I. In Fig. 5 (a), the SNR per symbol $\gamma_s$ at the BER of $10^{-4}$ required for the OFDM-LPIM system is plotted. Based on our previous study, we can now show that in order to attain a performance that is closer to Shannon capacity, the parameters of our proposed OFDM-LPIM scheme should be chosen based on Fig. 3. However, as shown in Fig. 5 (b), the corresponding price to pay is the associated complexity cost. In particular, we are interested in observing from Fig. 5 (a) that our LPIM codebook associated with $(m = 4, k = 2, Q = 4)$ performs closer to the Shannon capacity than the one using $(m = 4, k = 1, Q = 16)$, when the same maximum achievable rate $R_{\mathcal{V}_U} = 1.5$ bits/s/Hz and the same complexity cost shown in Fig. 5 (b). Thus, we may conclude that the optimal parameters of our proposed LPIM codebook should be chosen to strike a tradeoff between the distance from the Shannon capacity and the complexity cost.

Fig. 6 depicts the complementary cumulative distribution function (CCDF) of the number of iterations in the proposed GIRCD for the OFDM-LPIM system employing the depth-$G$ interleaver. Generally, CCDF represents the probability that

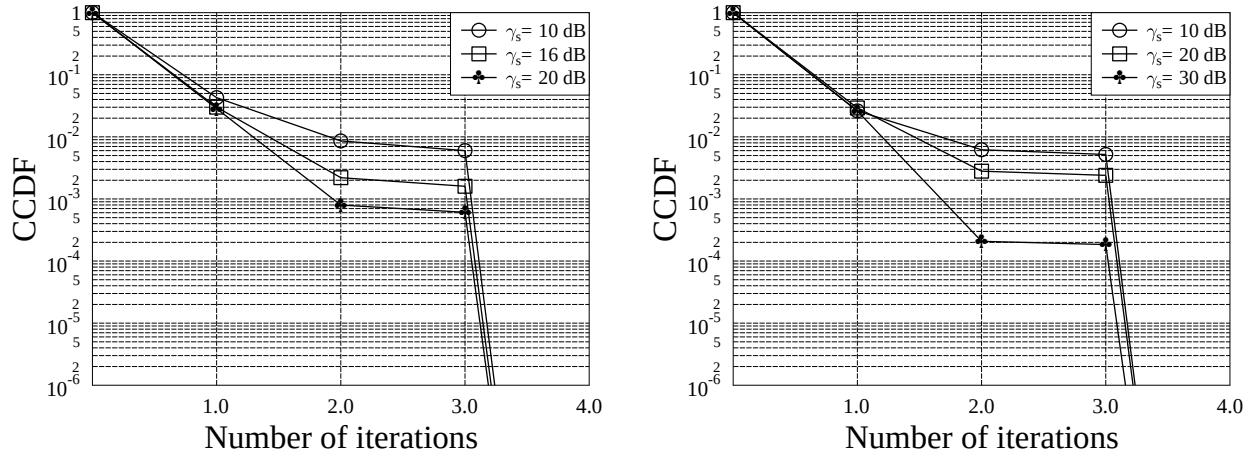


(a) (b)

Fig. 6: CCDF of the number of iterations of the GIRCD for the LPIM employing the depth-$G$ interleaver and operating at (a) $R_{\mathcal{V}_{\boldsymbol{U}}} = 1.5$ bits/s/Hz and $\gamma_s = 10$ dB, 16 dB or 20 dB; (b) $R_{\mathcal{V}_{\boldsymbol{U}}} = 2.5$ bits/s/Hz and $\gamma_s = 10$ dB, 20 dB or 30 dB. The rate $R_{\mathcal{V}_{\boldsymbol{U}}}$ is obtained based on (24).

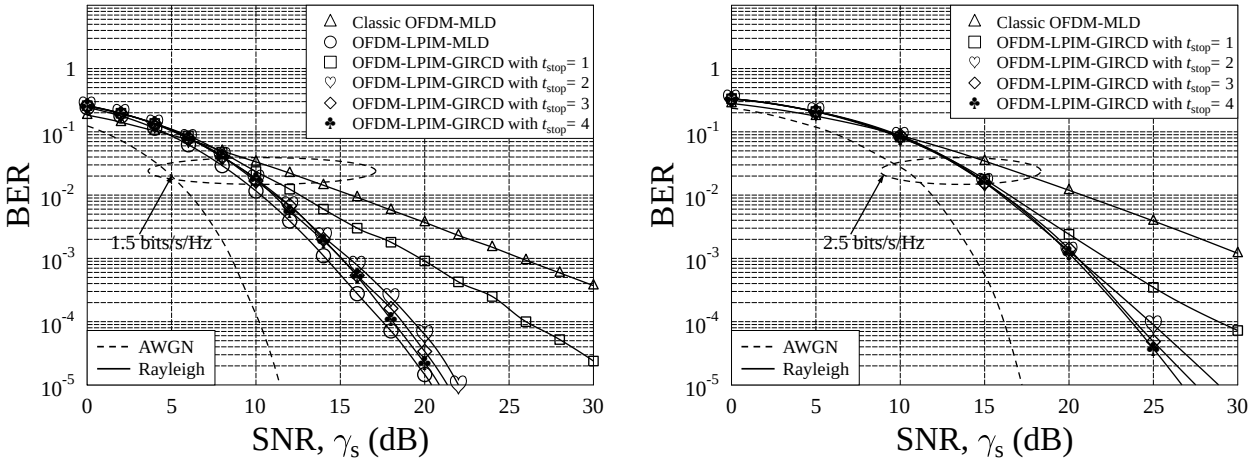


(a) (b)

Fig. 7: BER versus SNR for the OFDM-LPIM using JMLD and GIRCD. The OFDM-LPIM system employs the depth-$G$ interleaver and operates at 1.5 bits/s/Hz. For GIRCD shown in Algorithm 1, the maximum number of iterations is chosen to be $t_{\text{stop}} = 1$, 2, 3 or 4.

TABLE II: Simulation Results of Detection Complexity at 1.5 bits/s/Hz

| Codebook $\mathcal{V}$ | Parameters $(m, k, Q)$ | Complexity order of JMLD in dB | Complexity order of GIRCD in dB |
|---|---|---|---|
| LPIM $\mathcal{V}_{\boldsymbol{U}}$ | $(4, 2, 4)$ | 18.0618 | 12.1761 |

a random variable $X$ will take a value higher than $x$, i.e. we have $\text{CCDF}_X(x) \triangleq P(X > x)$. As shown in Fig. 6, the CCDF curves show a sharp decay as the number of iterations increases from zero to two. This observation implies that GIRCD is usually terminates in just a single iteration. For example, we can observe from Fig. 6 (a) that the probability of GIRCD terminates at iterations larger than one is about $7.5 \times 10^{-2}$. Furthermore, we can also observe from Fig. 6 that when GIRCD is restricted to be terminated at one iteration, the difference of the probabilities for GIRCD operating at different SNR per bit values is unnoticeable. In this case, the performance of GIRCD using a single iteration is stable at all SNR per bit values. Finally, we can also observe from Fig. 6 that as the EE of the proposed system increases, the probability of completing the detection process is increased only by one or two iterations. It should be noted that the complexity of our GIRCD is dependent on the number of iterations actually

invoked, rather than on the maximum number of iterations $t_{\text{stop}}$, as analyzed in Section V-C. Thus, our GIRCD can be deemed to be an efficient detector, since it usually terminates after a single or two iterations.

In Fig. 7, we compare the BER performance of both the joint maximum-likelihood detector (JMLD) and GIRCD designed for the OFDM-LPIM system. Specifically, the OFDM-LPIM systems are characterized by $(m = 4, k = 2, Q = 4)$ for $R_{\mathcal{V}_{\boldsymbol{U}}} = 1.5$ bits/s/Hz and by $(m = 4, k = 2, Q = 16)$ for $R_{\mathcal{V}_{\boldsymbol{U}}} = 2.5$ bits/s/Hz in Fig. 7 (a) and Fig. 7 (b), respectively. We observe from the results of Fig. 7 that the BER performance of the OFDM-LPIM system using our GIRCD invoking two iterations is stable for all SNR values. Furthermore, as seen in Fig. 7, a satisfactory BER performance is achievable for GIRCD using as few as two iterations. Here, it should be emphasized that the notation $t_{\text{stop}}$ serves as an upper bound of the number of iterations in our GIRCD of Algorithm 1. In fact, as shown in Fig. 6, our GIRCD usually terminates after just a single or two iterations, imposing a low-complexity. Moreover, as seen in Table II, our GIRCD is capable of providing a much lower complexity in comparison to the JMLD. This has two reasons. First, each index is uniquely tested, as shown in Algorithm 1. In this way, we avoid the repeated search process. The second reason can be understood by comparing (48) to (42), where the APM symbols are detected on a symbol-by-symbol basis by GIRCD, while the joint group detection is performed by the JMLD. Finally, based on the above observations, we can show that our proposed OFDM-LPIM system employing GIRCD can achieve a satisfactory BER performance associated with a high SE at a low complexity.

## VII. Conclusions

In this paper, a generalized system model and an unified performance analysis of OFDM-IM systems have been offered, where the bit-to-symbol mapping rule has been modeled as a codebook. Based on our theoretical analysis, the relevant codebook design criteria have been provided in terms of the diversity and coding gains. Then, an LPIM codebook has been proposed. Both our analytical and computer simulation results have shown that the proposed OFDM-LPIM scheme is capable of attaining a compelling BER performance. Finally, GIRCD schemes have been proposed for OFDM-LPIM to reduce the corresponding detection complexity. Simulation results have been provided for characterizing the overall system performance. Our investigations have demonstrated that OFDM-LPIM is capable of achieving a much better BER performance than the conventional OFDM-IM, despite its significantly reduced complexity. At a high rate, the OFDM-LPIM scheme using GIRCD has been shown to be still capable of attaining a satisfactory BER performance at a reduced complexity.

## Appendix

*Proof:* Here, it is convenient to rewrite the OFDM-IM symbol vector $\boldsymbol{x}_g$ given in (1) as $\boldsymbol{x}_g = \sqrt{\rho}\check{\boldsymbol{x}}_g$, where $\sqrt{\rho}$ is the constellation normalization factor. Then, we can model each symbol in $\check{\boldsymbol{x}}_g$ as a point from the ring of Gaussian integers, which is defined as $\mathbb{Z}[j] = \{a + jb : a, b \in \mathbb{Z}\}$. Explicitly, it can be readily shown that the activated symbols in $\check{\boldsymbol{x}}_g$ belong to $\mathbb{Z}[j]$, since they are drawn from the square QAM constellation. Moreover, we can also show that the zero-valued symbols in $\check{\boldsymbol{x}}_g$ correspond to the origin of $\mathbb{Z}[j]$. Similarly, we can point out that when the activated symbols in $\check{\boldsymbol{x}}_g$ are drawn from the triangular QAM/PSK constellation, each symbol in the OFDM-IM symbol vector $\check{\boldsymbol{x}}_g$ given in (1) can be modeled as a point from the ring of Eisenstein integers, which is defined as $\mathbb{Z}[\omega] = \{a + \omega b : a, b \in \mathbb{Z}\}$ with $\omega \triangleq \exp(j2\pi/3)$. Then, we can rewrite (25) as

$$\boldsymbol{e} = \boldsymbol{U}\left(\boldsymbol{x}_g^{\text{c}} - \boldsymbol{x}_g^{\text{e}}\right) = \sqrt{\rho}\boldsymbol{U}\left(\check{\boldsymbol{x}}_g^{\text{c}} - \check{\boldsymbol{x}}_g^{\text{e}}\right) = \sqrt{\rho}\boldsymbol{U}\boldsymbol{\chi}, \tag{51}$$

where, by definition, we have $\boldsymbol{\chi} \triangleq \check{\boldsymbol{x}}_g^{\text{c}} - \check{\boldsymbol{x}}_g^{\text{e}}$. It can be readily shown that each element in $\boldsymbol{\chi}$ can be also modeled as a point from $\mathbb{Z}[j]$ or $\mathbb{Z}[\omega]$. Moreover, according to the definition of $\boldsymbol{x}_g^{\text{c}}$ and $\boldsymbol{x}_g^{\text{e}}$ in (25), we can show that $\boldsymbol{\chi} \neq \boldsymbol{0}$. According to (35), the $i$th element of $\boldsymbol{e}$ can be expressed as

$$e(i) = \sqrt{\frac{\rho}{m}} \sum_{q=1}^{m} \left(\alpha_P^q\right)^{p_i} \chi(q). \tag{52}$$

By invoking *Theorem 1* in [24], we have

$$e(i) = \sqrt{\frac{\rho}{m}} \sum_{q=1}^{m} \sigma_i\left(\alpha_P^q\right) \chi(q), \tag{53}$$

where $\sigma_i(\alpha_P) = \alpha_P^{p_i}$ is the $i$th automorphism of the field $\mathbb{Q}(\alpha_P)$ over $\mathbb{Q}(\alpha_p)$ with $\gcd(p_i, P) = 1$ and $p_i = 1 + n_i p$ for $n_i = 0, \ldots, P/p$. It can be readily shown that when $\boldsymbol{\chi} = \boldsymbol{0}$, we have $e(i) = 0$. Since the $m$ automorphisms are distinct and each automorphism is a one-to-one mapping, we can show that for any $\boldsymbol{\chi} \neq \boldsymbol{0}$, we have $e(i) \neq 0$ for $i = 1, \ldots, m$. Thus, we have

$$\prod_{i=1}^{m} e(i) \neq 0, \tag{54}$$

which is equivalent to

$$\|\boldsymbol{e}\|_0 = m, \tag{55}$$

meaning that The codebook $\mathcal{V}_{\boldsymbol{U}}$ associated with the LP matrix of (35) achieves the full diversity order. ■

## Acknowledgment

The authors would like to thank the Editor and the anonymous reviewers for their useful comments and insightful suggestions to improve the quality of this manuscript.

## References

[1] M. Di Renzo, H. Haas, A. Ghrayeb, S. Sugiura and L. Hanzo, "Spatial modulation for generalized MIMO: Challenges, opportunities, and implementation," *Proceedings of the IEEE*, vol. 102, no. 1, pp. 56–103, Jan 2014.

[2] E. Basar, "Index modulation techniques for 5G wireless networks," *IEEE Communications Magazine*, vol. 54, no. 7, pp. 168–175, July 2016.

[3] M. Wen, X. Cheng, and L. Yang, *Index Modulation for 5G Wireless Communications*. Springer, 2016.

[4] R. Abu-alhiga and H. Haas, "Subcarrier-index modulation OFDM," in *2009 IEEE 20th International Symposium on Personal, Indoor and Mobile Radio Communications*, Sept 2009, pp. 177–181.

[5] D. Tsonev, S. Sinanovic and H. Haas, "Enhanced subcarrier index modulation (SIM) OFDM," in *2011 IEEE GLOBECOM Workshops (GC Wkshps)*, Dec 2011, pp. 728–732.
[6] E. Basar, U. Aygolu, E. Panayirci and H. V. Poor, "Orthogonal frequency division multiplexing with index modulation," *IEEE Transactions on Signal Processing*, vol. 61, no. 22, pp. 5536–5549, Nov 2013.
[7] M. Wen, X. Cheng and L. Yang, "Optimizing the energy efficiency of OFDM with index modulation," in *2014 IEEE International Conference on Communication Systems (ICCS)*, Nov 2014, pp. 31–35.
[8] M. Wen, X. Cheng, M. Ma, B. Jiao, and H. V. Poor, "On the achievable rate of OFDM with index modulation," *IEEE Transactions on Signal Processing*, vol. 64, no. 8, pp. 1919–1932, April 2016.
[9] H. Zhang, L. L. Yang, and L. Hanzo, "Compressed sensing improves the performance of subcarrier index-modulation-assisted OFDM," *IEEE Access*, vol. 4, pp. 7859–7873, 2016.
[10] H. Zhang, L. L. Yang and L. Hanzo, "LDPC-coded index-modulation aided OFDM for in-vehicle power line communications," in *2016 IEEE 83rd Vehicular Technology Conference (VTC Spring)*, May 2016, pp. 1–5.
[11] R. Fan, Y. J. Yu, and Y. L. Guan, "Generalization of orthogonal frequency division multiplexing with index modulation," *IEEE Transactions on Wireless Communications*, vol. 14, no. 10, pp. 5350–5359, 2015.
[12] T. Mao, Z. Wang, Q. Wang, S. Chen, and L. Hanzo, "Dual-mode index modulation aided OFDM," *IEEE Access*, vol. 5, pp. 50–60, 2017.
[13] T. Mao, Q. Wang, and Z. Wang, "Generalized dual-mode index modulation aided OFDM," *IEEE Communications Letters*, vol. 21, no. 4, pp. 761–764, 2017.
[14] M. Wen, E. Basar, Q. Li, B. Zheng, and M. Zhang, "Multiple-mode orthogonal frequency division multiplexing with index modulation," *IEEE Transactions on Communications*, vol. 65, no. 9, pp. 3892–3906, 2017.
[15] E. Basar, "OFDM with index modulation using coordinate interleaving," *IEEE Wireless Communications Letters*, vol. 4, no. 4, pp. 381–384, Aug 2015.
[16] N. Ishikawa, S. Sugiura, and L. Hanzo, "Subcarrier-index modulation aided OFDM - will it work?" *IEEE Access*, vol. 4, pp. 2580–2593, 2016.
[17] Y. Xiao *et al.*, "OFDM with interleaved subcarrier-index modulation," *IEEE Communications Letters*, vol. 18, no. 8, pp. 1447–1450, Aug 2014.
[18] A. Khan, M.Z. and B. S. Rajan, "Single-symbol maximum likelihood decodable linear STBCs," *IEEE Transactions on Information Theory*, vol. 52, no. 5, pp. 2062–2091, May 2006.
[19] J. Zheng and R. Chen, "Achieving transmit diversity in OFDM-IM by utilizing multiple signal constellations," *IEEE Access*, vol. 5, pp. 8978–8988, 2017.
[20] M. Wen, B. Ye, E. Basar, Q. Li, and F. Ji, "Enhanced orthogonal frequency division multiplexing with index modulation," *IEEE Trans. Wireless Commun.*, vol. 16, no. 7, pp. 4786–4801, 2017.
[21] V. Tarokh, N. Seshadri and A. R. Calderbank, "Space-time codes for high data rate wireless communication: performance criterion and code construction," *IEEE Transactions on Information Theory*, vol. 44, no. 2, pp. 744–765, Mar 1998.
[22] J. Boutros and E. Viterbo, "Signal space diversity: a power- and bandwidth-efficient diversity technique for the Rayleigh fading channel," *IEEE Transactions on Information Theory*, vol. 44, no. 4, pp. 1453–1467, Jul 1998.
[23] Y. Xin, Z. Wang, and G. B. Giannakis, "Space-time diversity systems based on linear constellation precoding," *IEEE Transactions on Wireless Communications*, vol. 2, no. 2, pp. 294–309, Mar 2003.
[24] G. Wang, H. Liao, H. Wang, and X.-G. Xia, "Systematic and optimal cyclotomic lattices and diagonal space-time block code designs," *IEEE Transactions on Information Theory*, vol. 50, no. 12, pp. 3348–3360, Dec 2004.
[25] W. Su, Z. Safar, and K. J. R. Liu, "Full-rate full-diversity space-frequency codes with optimum coding advantage," *IEEE Transactions on Information Theory*, vol. 51, no. 1, pp. 229–249, Jan 2005.
[26] L. Hanzo, M. El-Hajjar and O. Alamri, "Near-capacity wireless transceivers and cooperative communications in the MIMO era: Evolution of standards, waveform design, and future perspectives," *Proceedings of the IEEE*, vol. 99, no. 8, pp. 1343–1385, Aug 2011.
[27] S. Sugiura, S. Chen, and L. Hanzo, "Coherent and differential space-time shift keying: A dispersion matrix approach," *IEEE Transactions on Communications*, vol. 58, no. 11, pp. 3219–3230, November 2010.
[28] L. L. Yang, "Signal detection in antenna-hopping space-division multiple-access systems with space-shift keying modulation," *IEEE Transactions on Signal Processing*, vol. 60, no. 1, pp. 351–366, Jan 2012.
[29] J. Boutros, E. Viterbo, C. Rastello, and J. C. Belfiore, "Good lattice constellations for both Rayleigh fading and Gaussian channels," *IEEE Transactions on Information Theory*, vol. 42, no. 2, pp. 502–518, Mar 1996.
[30] Z. Liu, Y. Xin and G. B. Giannakis, "Linear constellation precoding for OFDM with maximum multipath diversity and coding gains," *IEEE Transactions on Communications*, vol. 51, no. 3, pp. 416–427, March 2003.
[31] N. H. Tran, H. H. Nguyen, and T. Le-Ngoc, "Bit-interleaved coded OFDM with signal space diversity: Subcarrier grouping and rotation matrix design," *IEEE Transactions on Signal Processing*, vol. 55, no. 3, pp. 1137–1149, March 2007.
[32] Z. Liu, "Maximum diversity in single-carrier frequency-domain equalization," *IEEE Transactions on Information Theory,*, vol. 51, no. 8, pp. 2937–2940, Aug 2005.
[33] N. Prasad, L. Venturino, and X. Wang, "Diversity-multiplexing tradeoff analysis for OFDM systems with subcarrier grouping, linear precoding, and linear detection," *IEEE Transactions on Information Theory*, vol. 56, no. 12, pp. 6078–6096, Dec 2010.
[34] J. Zhang, L. L. Yang, L. Hanzo, and H. Gharavi, "Advances in cooperative single-carrier FDMA communications: Beyond LTE-advanced," *IEEE Communications Surveys Tutorials*, vol. 17, no. 2, pp. 730–756, Secondquarter 2015.
[35] B. Zhu, J. Cheng, J. Yan, J. Wang, L. Wu, and Y. Wang, "A new asymptotic analysis technique for diversity receptions over correlated lognormal fading channels," *IEEE Transactions on Communications*, 2017.
[36] X. Giraud, E. Boutillon, and J. C. Belfiore, "Algebraic tools to build modulation schemes for fading channels," *IEEE Transactions on Information Theory*, vol. 43, no. 3, pp. 938–952, May 1997.
[37] S. G. Mallat and Z. Zhang, "Matching pursuits with time-frequency dictionaries," *IEEE Transactions on Signal Processing*, vol. 41, no. 12, pp. 3397–3415, Dec 1993.
[38] D. Needell and J. A. Tropp, "CoSaMP: Iterative signal recovery from incomplete and inaccurate samples," *Applied and Computational Harmonic Analysis*, vol. 26, no. 3, pp. 301–321, 2009.
[39] L.-L. Yang, "Receiver multiuser diversity aided multi-stage minimum mean-square error detection for heavily loaded DS-CDMA and SDMA systems," *IEEE Transactions on Communications*, vol. 58, no. 12, pp. 3397–3404, December 2010.